Broadband Nonreciprocal Amplification in Luminal Metamaterials

E. Galiffi,[1] P. A. Huidobro,[2] and J. B. Pendry[1]
[1]Condensed Matter Theory Group, The Blackett Laboratory, SW72AZ Imperial College London, United Kingdom
[2]Instituto de Telecomunicações, Instituto Superior Tecnico-University of Lisbon, Avenida Rovisco Pais 1,1049-001 Lisboa, Portugal

(Received 6 July 2019; published 15 November 2019)

Time has emerged as a new degree of freedom for metamaterials, promising new pathways in wave control. However, electromagnetism suffers from limitations in the modulation speed of material parameters. Here we argue that these limitations can be circumvented by introducing a traveling-wave modulation, with the same phase velocity of the waves. We show how luminal metamaterials generalize the parametric oscillator concept, realize giant broadband nonreciprocity, achieve efficient one-way amplification, pulse compression, and harmonic generation, and propose a realistic implementation in double-layer graphene.

DOI: 10.1103/PhysRevLett.123.206101

Temporal control of light is a long-standing dream, which has recently demonstrated its potential to revolutionize optical and microwave technology, as well as our understanding of electromagnetic theory, overcoming the stringent constraint of energy conservation [1]. Along with the ability of time-dependent systems to violate electromagnetic reciprocity [2–4], realize photonic isolators and circulators [5–8], amplify signals [9], and perform harmonic generation [10–12] and phase modulation [13], new concepts from topological [14–16] and non-Hermitian physics [17,18] are steadily permeating this field. However, current limitations to the possibility of significantly fast modulation in optics has constrained the concept of time-dependent electromagnetics to the radio frequency domain, where varactors can be used to modulate capacitance [19], and traveling-wave tubes are commonly used as (bulky) microwave amplifiers [20]. In the visible and near IR, optical nonlinearities have often been exploited to generate harmonics and realize certain nonreciprocal effects [21]. However, nonlinearity is an inherently weak effect, and high field intensities are typically required.

In this Letter, we challenge the very need for high modulation frequencies, demonstrating that strong and broadband nonreciprocal response can be obtained by complementing the temporal periodic modulation of an electromagnetic medium with a spatial one, in such a way that the resulting traveling-wave modulation profile appears to drift uniformly at the speed of the wave, i.e., a "luminal" modulation. We show that unidirectional amplification and compression can be accomplished in luminal metamaterials, which thus constitute a broadband generalization of the narrow-band concept of the parametric oscillator, enabling harmonic generation with exponential efficiency. We present a realistic implementation based on acoustic plasmons in double-layer graphene (DLG), thus circumventing the intrinsic limitations in the modulation speed of its doping level. Our findings, which are transferable to other wave domains, hold potential for efficient harmonic generation (terahertz, in the specific case of graphene), loss compensation, and amplification of waves.

Bloch (Floquet) theory dictates that the wave vector (frequency) of a monochromatic wave propagating in a spatially (temporally) periodic medium can only Bragg scatter onto a discrete set of harmonics, determined by the reciprocal lattice vectors. This still holds true when the modulation is of a traveling-wave type, whereby Bragg scattering couples Fourier modes, which differ by a discrete amount of both energy and momentum [2,7,22–25]. As shown in Fig. 1 for a 1D system, these space-time reciprocal lattice vectors can be defined to take any angle in phase space, depending on whether a generic traveling-wave modulation of the material parameters of the form $\delta\epsilon(gx - \Omega t)$ is spatial [Fig. 1(a) $\Omega = 0$], temporal [Fig. 1(d) $g = 0$], or spatiotemporal [Figs. 1(b) and 1(c) $g \neq 0$, $\Omega \neq 0$]. Given the slope c_0 of the bands in a Brillouin diagram, which denotes the velocity of waves in a dispersionless medium, the speed of the traveling-wave modulation defines a subluminal regime $\Omega/g < c_0$ [Figs. 1(a) and 1(b)], whereby conventional vertical band gaps open [22], and a superluminal one $\Omega/g > c_0$ [Figs. 1(c) and 1(d)], characterized by horizontal, unstable k gaps [23,26]. A common example of the latter is the parametric amplifier [$g = 0$, Fig. 1(d)]: when the parameters governing an oscillatory system are periodically driven at twice its natural frequency, exponential amplification occurs, as a result of the unstable k gap at frequency $\omega = \Omega/2$. However, achieving such fast modulation at infrared frequencies remains a key challenge for dynamical metamaterials.

The transition between the regimes in Figs. 1(b) and 1(c), i.e., $\Omega/g = c_0$, is an exotic degenerate state that we name luminal metamaterial, whereby all forward-propagating modes are uniformly coupled. Because of its broadband

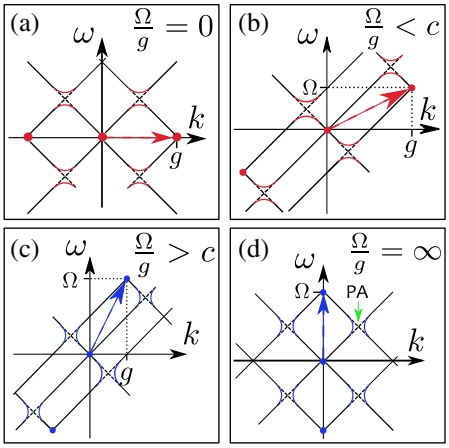

FIG. 1. (a) The band structure of a conventional spatial crystal is repeated in phase space at $k = ng$, $n \in \mathbb{Z}$, forming vertical band gaps (ω gaps). (b) Similarly, the band structure of a traveling-wave-modulated crystal is symmetric under discrete translations by an oblique reciprocal lattice vector (g, Ω). When $\Omega/g < c_0$, ω gaps open, whereas (c) $\Omega/g > c_0$ leads to unstable k gaps. (d) Finally, if the wavelength of the modulation $L \to \infty$, then $g \to 0$, so that the system is effectively only modulated in time. In this case, the modulation speed $\Omega/g \to \infty$ and the system becomes a narrow-band, reciprocal, parametric amplifier. The transition between (b) and (c), whereby the light line and the reciprocal lattice vector are aligned, is a luminal crystal.

spectral degeneracy in the absence of dispersion, this system is highly unstable, thus preventing a meaningful definition of its band structure. Nevertheless, if we consider transmission through a spatially (temporally) finite system with well-defined boundary conditions, causality can be imposed in the unmodulated regions of space (time), so that an expansion into eigenfunctions can be performed, as detailed in the Supplemental Material [27]. In luminal metamaterials, the photonic transitions induced by the modulation of the refractive index are no longer interband [31], but intraband, and can therefore be driven by means of any refractive index modulation, regardless of how adiabatic, whose reciprocal lattice vector (g, Ω) satisfies the speed-matching condition $\Omega/g = c_0$. Hence, any limitation in modulation frequency Ω can be compensated, in principle, by a longer spatial period $L = 2\pi/g$. Notably, these can be locally induced by modulating the properties of the medium and can thus synthetically move at any speed, including and exceeding the speed of light, in analogy with the touching point of a water wave front propagating almost perpendicularly to a beach or the junction between the blades of a pair of scissors.

In real space, amplification in this system can be modeled as follows: consider a nondispersive, lossless medium where $\varepsilon(x,t) = 1 + 2\alpha\cos(gx - \Omega t)$, with $\Omega/g = c_0$. Following the derivation of Poynting's theorem, we can write

$$\nabla \cdot (\mathbf{E} \times \mathbf{H}) = -\frac{\mu_0}{2}\frac{\partial H^2}{\partial t} - \frac{\varepsilon_0 \varepsilon}{2}\frac{\partial E^2}{\partial t} - \varepsilon_0 \frac{\partial \varepsilon}{\partial t} E^2, \quad (1)$$

so that the total time derivative of the local energy density is

$$\frac{dU}{dt} = -\frac{1}{\varepsilon}\frac{\partial \varepsilon}{\partial t} U - \frac{\partial P}{\partial x} + c_0 \frac{\partial U}{\partial x} = -\frac{1}{\varepsilon}\frac{\partial \varepsilon}{\partial t} U - \frac{\partial P'}{\partial x}, \quad (2)$$

where the compensated Poynting vector P' consists of a local and an advective part (due to the moving frame) [27]. The first term in Eq. (2) is responsible for gain, whereas the second describes the Poynting flux, which drives the compression of the pulse. Ignoring the Poynting contribution to zero order yields $U(X,t) = e^{-2\alpha\Omega t \sin(gX)}$, where $X = x - \Omega t/g$. Feeding the zero-order solution into the resulting compensated Poynting vector $P' = c_0[\varepsilon(X,t)^{-1/2} - 1]U$ in Eq. (2), we obtain a corrected expression for the energy density

$$U(X,t) = \exp\left[-2\alpha\Omega t \sin(gX) - \alpha^2\Omega^2 t^2 \cos^2(gX)\right]. \quad (3)$$

Alternatively, the system can also be modeled with a semianalytic Floquet-Bloch expansion of the fields, and the transmission coefficient can be calculated for a finite slab, validating our analytical expressions [27]. Assuming a slab of length d, and substituting $\Omega t = gd$ in Eq. (3), we calculate the temporal profile of the electric field intensity at the output $x = d$ [Fig. 2(a)]. The modulation is able to exponentially amplify and concentrate the signal at the point with phase $\Omega t = \pi/2$ and exponentially suppress it at $\Omega t = 3\pi/2$. The reason is apparent from Fig. 2(b): those field amplitudes that sit at $-\pi/2 < \Omega t < \pi/2$ experience a lower permittivity, and hence a higher phase velocity, whereas those sitting at $\pi/2 < \Omega t < 3\pi/2$ lag, so that the point corresponding to a phase $\Omega t = \pi/2$ acts as an attractor, or gain point, where the modulation imparts energy into the wave. Conversely, $\Omega t = 3\pi/2$ is a repeller, or loss point, where energy is absorbed by the modulation drive (further numerical simulations are provided in the Supplemental Material [27]).

As evidenced by the absence of any frequency dependence in Eq. (3), and in contrast to conventional time-modulated systems, parametric amplification in a luminal medium is a fully broadband phenomenon, enabling exponentially efficient generation of frequency wave-vector harmonics, as shown in Fig. 2(c). Remarkably, even a dc input can be transformed into a broadband pulse train at an exponential rate, as revealed by Floquet-Bloch calculations [see Fig. 2(d)]. Our closed-form analytic solution enables us to exactly quantify the power amplification rate as $2\alpha\Omega$, which needs to overcome the loss for amplification to occur. However, the reactive behavior responsible for the compression performance is unaffected by losses, which only reduce the overall output power efficiency. Furthermore, these systems are transparent to

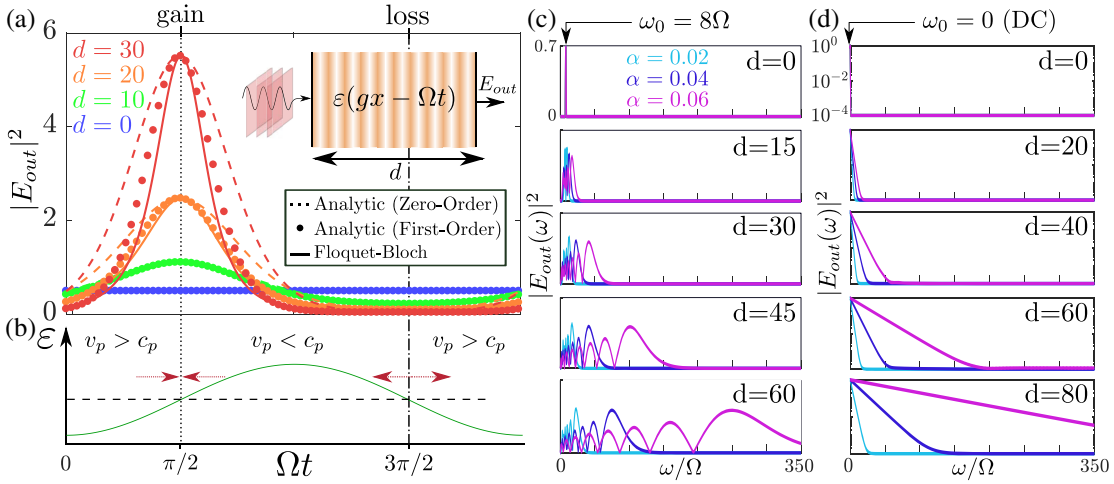

FIG. 2. (a) An incident plane wave is concentrated and exponentially amplified as it propagates through a luminal metamaterial ($g = \Omega = 1$, $\alpha = 0.04$) of length d (inset), at whose exit the field is calculated. Continuous lines correspond to Floquet-Bloch theory, whereas dashed lines and circles were obtained from our analytic model to zeroth and first [Eq. (3)] order, respectively. (b) Waves preceding (following) the gain point ($\Omega t = \pi/2$) experience a lower (higher) permittivity, hence a higher (lower) phase velocity, thus being attracted toward the gain point, at which amplification occurs. Conversely, waves preceding (following) the loss point ($\Omega t = 3\pi/2$) are drawn away from it, depleting it of energy. (c) An incident monochromatic wave with input frequency $\omega_0 = 8\Omega$ is efficiently coupled to higher harmonics at an exponential rate. Beating arises from the different Ω and ω_0. (d) The frequency content (log scale) of a dc input applied to a luminal metamaterial spreads out exponentially in Fourier space, generating a supercontinuum.

counterpropagating waves, thus entailing the additional advantage of nonreciprocity. Moreover, while nonreciprocal response is typically observed only near band gaps in conventional systems [2], it is achieved at virtually any frequency in a luminal metamaterial.

Because of their ease of manipulation, metasurfaces offer the most promising playground to realize dynamical effects [1,32,33], also due to the rise of tunable two-dimensional materials [34,35]. Recently, graphene has emerged as a platform to enhance light-matter interactions [36–39], realizing atomically thin metasurfaces [13,40–43]. Its doping level, which can be tuned with ion-gel techniques to be as high as 2 eV [44,45], can be dynamically modulated via all-optical techniques, with experimentally reported response times as short as 2.2 ps at relative doping modulation amplitudes of 38% [46,47]. In addition, modern-quality graphene features extremely high electron mobility, with measured experimental values of 350 000 $\mathrm{cm}^2/(\mathrm{V\,s})$ [48].

The dispersion relation of graphene plasmons follows a square root behavior $\omega \sim \sqrt{k}$, where ω is the angular frequency and k is the in-plane wave vector. However, in a double-layer configuration [Fig. 3(a)], a second "acoustic" plasmon branch arises [28,49,50], whose dispersion

$$\omega \propto \sqrt{\epsilon_F}\sqrt{k(1-e^{-\delta_0 k})} \simeq \sqrt{\delta_0 \epsilon_F}k\left(1-\frac{\delta_0 k}{4}\right) \quad (4)$$

is linear for small interlayer gaps $\delta_0 \ll k^{-1}$ (ϵ_F is the Fermi energy). Here we exploit the linearity of this acoustic plasmon band to realize a luminal metasurface, while accounting for dispersion, and we demonstrate nonreciprocal plasmon amplification and compression. Alternative amplification schemes for graphene plasmons have been theoretically proposed, such as drift currents [51–53], periodic doping modulation [54], adiabatic doping suppression [55], and plasmonic Čerenkov emission by hot carriers [56].

We assume a semiclassical (Drude) conductivity model, which is accurate as long as $\hbar\omega \ll \epsilon_F$ and $k \ll k_F$. Our setup consists of two graphene layers, whose Fermi levels are modulated as $\epsilon_F(x,t) = \epsilon_{F,0}[1 + 2\alpha\cos(gx - \Omega t)]$ [Fig. 3(a)]. Dispersion is accounted for by expressing the constitutive relation for the current $J(x,t)$ in Fourier space, where the conductivity modulation couples neighboring frequency harmonics

$$J_n = \frac{e^2\epsilon_{F,0}}{\pi\hbar^2}\frac{E_n + \alpha(E_{n+1} + E_{n-1})}{\gamma - i(\omega + n\Omega)}, \quad (5)$$

where γ is the loss rate and E_n is the nth Fourier amplitude of the in-plane electric field, which is continuous at the layer positions $z = 0$ and $z = \delta_0$, as detailed in the Supplemental Material [27]. The magnetic field of the p-polarized wave $H_y(x,z,t)$ is discontinuous at the layers by the surface current [28]. This system can be accurately described within an adiabatic regime, since the modulation frequency $\Omega \ll \omega$. Furthermore, since acoustic plasmons carry much larger momentum than photons, the modes are strongly quasistatic, so that the out-of-plane

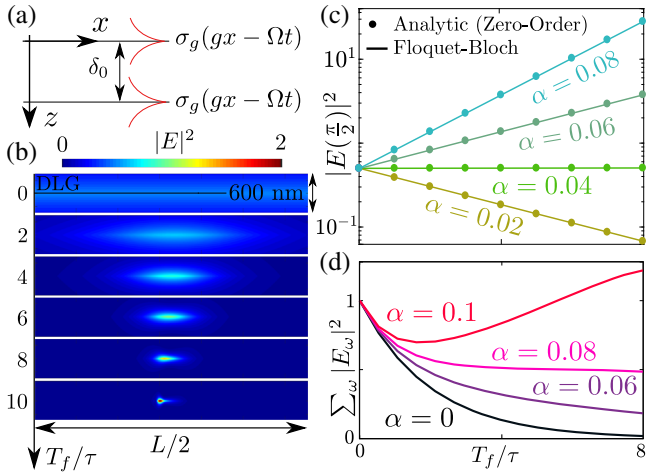

FIG. 3. (a) Double-layer graphene configuration. (b) The DLG plasmon intensity is amplified and compressed at the gain point $gX=\pi/2$, as a luminal modulation is applied over increasingly long time windows T_f. (c) The intensity at the gain point grows exponentially as a function of both modulation time T_f and amplitude α for sufficiently strong ($\alpha=0.06,\ 0.08$) or fast modulation, as predicted by our analytic model. (d) The integrated power of the plasmon reduces initially, due to dissipation. Once the pulse is localized near the gain point, loss compensation ($\alpha=0.06,\ 0.08$) and even amplification ($\alpha=0.1$) are possible.

decay constant $\kappa_n \simeq k+ng$, and coupling to radiation is negligible, given that both spatial and temporal frequencies of the doping modulation are much smaller than the plasmon wave vector and frequency. Taking advantage of the adiabatic assumption, we can conveniently solve the scattering problem in the time domain, as detailed in the Supplemental Material [27].

In our calculations, we assume a Fermi energy $\epsilon_F = 1.5\ \text{eV} \approx 2\pi\hbar \times 362\ \text{THz}$ and a loss rate $\gamma = (v_F^2 e/m\epsilon_{F,0}) \approx 60\ \text{GHz}$, where $m = 10^5\ \text{cm}^2/(\text{V s})$ is the electron mobility, and the Fermi velocity $v_F \approx 9.5\times 10^5\ \text{ms}^{-1}$. Figure 3(b) demonstrates plasmon amplification and compression for different modulation times T_f. Here, we use a modulation amplitude $\alpha=0.05$, interlayer gap $\delta_0 = 1$ nm, an input frequency $\omega/2\pi = 1$ THz, and a modulation frequency $\Omega/2\pi = 120$ GHz, which corresponds to a modulation period $\tau = 2\pi/\Omega \approx 8$ ps and length $L \approx 26\ \mu$m, such that the long-wavelength phase velocity of the plasmon is matched by the modulation speed $c_p = \Omega/g$. Since the DLG plasmon bands are approximately linear, we can set $c_0 = c_p$ in order to use our closed-form solution [Eq. (3)], and verify the analogous amplification mechanism, showing excellent agreement with Floquet-Bloch theory [Fig. 3(c)]. Finally, Fig. 3(d) demonstrates the total power amplification achieved by our luminal graphene metasurface: initially the unit input power of the wave is predominantly dissipated by the uniform losses, except at the gain point, so that this first propagation moment is dominated by damping. Once sufficient power is accumulated at the gain point, the energy fed by the modulation into the plasmon ensures that its propagation is effectively loss compensated, as in the case of $\alpha=0.08$, extending its lifetime by orders of magnitude, or even amplifying it, as in the $\alpha=0.1$ case.

As the luminal modulation couples the frequency content of the pulse to very high-frequency-wave-vector harmonics, these will experience the nonlinearity of the bands. In Fig. 4, we use a wider interlayer gap $\delta_0 = 15$ nm and higher mobility $m = 10^6\ \text{cm}^2/(\text{V s})$, to highlight the effects of dispersion on the pulse profile [Fig. 4(a)] and its spectral content [Fig. 4(b)] for different modulation times T_f. At a first stage, since higher frequency components experience a slightly lower phase velocity, the gain point must shift back to $gX < \pi/2$, where the increase in local phase velocity determined by the modulated Fermi energy compensates for the curvature of the band (Fig. 4, inset). In addition, Fourier components propagating with phase velocity c_p are amplified near the conventional gain point, thus skewing the pulse ($T_f = 5\tau$). Finally, for even longer propagation times, the wave will cease to compress and break into a train of pulses. This is due to the existence of a finite regime of phase velocities: $(1+2\alpha)^{-1/2} < v_p/c_p < (1-2\alpha)^{-1/2}$, within which the interaction between copropagating bands is strong enough

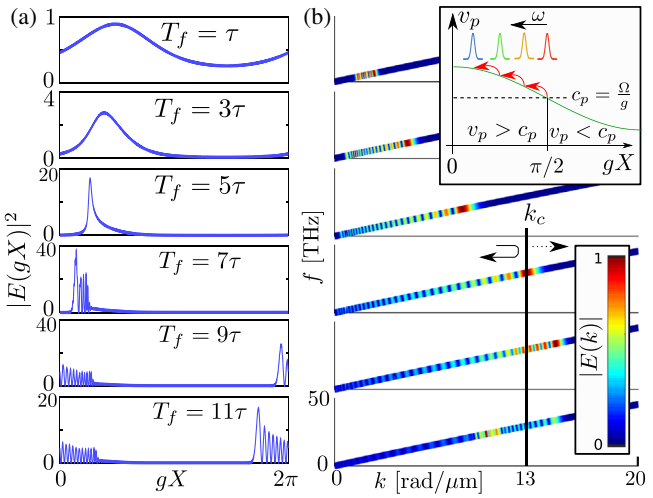

FIG. 4. (a) The effect of dispersion causes a gradual shift of the gain point due to the slower phase velocity of higher frequency components, as well as a skewing on the pulse. For even longer modulation times, the wave breaks into a train of narrow pulses. (b) The spectral content of the pulse is amplified and projected from an input frequency of ≈4 to ≈30 THz, demonstrating efficient terahertz frequency generation using a modulation frequency of only $\Omega/2\pi = 120$ GHz. High-frequency components whose phase velocity is below the instability threshold are not coupled; hence dispersion stabilizes the system. Here we assumed a wider gap $\delta_0 = 15$ nm to highlight the effect of dispersion, $\alpha = 0.05$.

to make the system unstable [23]. In our setup, the relative phase velocity

$$\frac{v_p(k)}{c_p} = \left(\frac{\omega(k)}{k}\right) \Big/ \left(\frac{\Omega}{g}\right) \simeq \left(\frac{1 - e^{-k\delta_0}}{\delta_0 k}\right)^{1/2} \tag{6}$$

decreases approximately linearly with increasing wave vector [27]. Equating the latter to the lower threshold velocity ratio $v_p(k_c)/c_p = 1/\sqrt{1+2\alpha}$, where $\alpha = 0.05$ and expanding the exponential to second order, we get an analytical estimate for the critical wave vector $k_c \approx 13\ \mathrm{rad}/\mu\mathrm{m}$, beyond which the pulse is no longer strongly excited to higher harmonics, and its power spectrum is effectively reflected, resulting in beating. Thus, dispersion plays the important role of stabilizing these systems. Subsequently, the power spectrum oscillates within the extended luminal region, although beating between different space-time harmonics, no longer in phase, induces fast oscillations, reminiscent of comb formation in nonlinear optics [57].

In this Letter, we have introduced the concept of luminal metamaterials, realized by inducing a traveling-wave modulation in the permittivity of a material, whose phase velocity matches that of the waves propagating in it, in the absence of modulation. We have shown that these dynamical structures generalize the concept of parametric amplification to cover a virtually unlimited bandwidth, thus being capable of reinforcing and compressing input waves of any frequency, including a dc field. We have demonstrated their robustness against moderate dispersion and proposed a realistic implementation exploiting acoustic plasmons in double-layer graphene, thus paving a new viable route toward the amplification of graphene plasmons and terahertz generation. Furthermore, luminal metamaterials exhibit an inherent, strongly nonreciprocal response at any frequency, due to the directional bias induced by the modulation, whose phase velocity can be made as high as needed by extending the spatial period of the modulation, the only limitation being the propagation length of the excitation, and hence the loss.

Furthermore, thanks to its ability to couple incident electromagnetic waves to higher frequency-momentum harmonics at an exponential rate, the luminal metamaterial concept constitutes a fundamentally new path toward efficient harmonic generation, which can work even with a dc input, necessitating only low modulation speeds, as opposed to conventional parametric systems. Finally, we remark that this concept can be translated to any wave system that exhibits a linear or weakly dispersive regime, such as acoustic, elastic, and shallow-water waves, and the reach of this mechanism could be further extended by introducing chirping, in analogy with the tuning of the frequency of a driving field with the energy of electrons accelerated in a synchrocyclotron.

E. G. acknowledges support through a studentship in the Centre for Doctoral Training on Theory and Simulation of Materials at Imperial College London funded by the EPSRC (EP/L015579/1). P. A. H. acknowledges funding from Fundação para a Ciência e a Tecnologia and Instituto de Telecomunicações under projects CEECIND/03866/2017 and UID/EEA/50008/2019. J. B. P. acknowledges funding from the Gordon and Betty Moore Foundation.

[1] A. M. Shaltout, V. M. Shalaev, and M. L. Brongersma, Science **364**, eaat3100 (2019).
[2] D. L. Sounas and A. Alù, Nat. Photonics **11**, 774 (2017).
[3] Y. Hadad, J. C. Soric, and A. Alu, Proc. Natl. Acad. Sci. U.S.A. **113**, 3471 (2016).
[4] C. Caloz, A. Alù, S. Tretyakov, D. Sounas, K. Achouri, and Z.-L. Deck-Léger, Phys. Rev. Applied **10**, 047001 (2018).
[5] D.-W. Wang, H.-T. Zhou, M.-J. Guo, J.-X. Zhang, J. Evers, and S.-Y. Zhu, Phys. Rev. Lett. **110**, 093901 (2013).
[6] D. L. Sounas, C. Caloz, and A. Alu, Nat. Commun. **4**, 2407 (2013).
[7] Z. Yu and S. Fan, Nat. Photonics **3**, 91 (2009).
[8] K. Fang, Z. Yu, and S. Fan, Phys. Rev. Lett. **108**, 153901 (2012).
[9] T. T. Koutserimpas, A. Alù, and R. Fleury, Phys. Rev. A **97**, 013839 (2018).
[10] N. Chamanara and C. Caloz, arXiv:1810.04129.
[11] Z.-L. Deck-Léger, N. Chamanara, M. Skorobogatiy, M. G. Silveirinha, and C. Caloz, arXiv:1808.02863.
[12] V. Ginis, P. Tassin, T. Koschny, and C. M. Soukoulis, Phys. Rev. B **91**, 161403(R) (2015).
[13] M. C. Sherrott, P. W. Hon, K. T. Fountaine, J. C. Garcia, S. M. Ponti, V. W. Brar, L. A. Sweatlock, and H. A. Atwater, Nano Lett. **17**, 3027 (2017).
[14] Q. Lin, M. Xiao, L. Yuan, and S. Fan, Nat. Commun. **7**, 13731 (2016).
[15] R. Fleury, A. B. Khanikaev, and A. Alu, Nat. Commun. **7**, 11744 (2016).
[16] L. He, Z. Addison, J. Jin, E. J. Mele, S. G. Johnson, and B. Zhen, Nat. Commun. **10**, 4194 (2019).
[17] T. T. Koutserimpas and R. Fleury, Phys. Rev. Lett. **120**, 087401 (2018).
[18] A. Regensburger, C. Bersch, M.-A. Miri, G. Onishchukov, D. N. Christodoulides, and U. Peschel, Nature (London) **488**, 167 (2012).
[19] S. H. Barnes and J. E. Mann, U.S. Patent No. 2,**989**, 671 (1961).
[20] J. R. Pierce, Bell Syst. Tech. J. **29**, 189 (1950).
[21] D. L. Sounas, J. Soric, and A. Alu, National electronics review **1**, 113 (2018).
[22] E. Cassedy and A. Oliner, Proc. IEEE **51**, 1342 (1963).
[23] E. Cassedy, Proc. IEEE **55**, 1154 (1967).
[24] F. Biancalana, A. Amann, A. V. Uskov, and E. P. O'Reilly, Phys. Rev. E **75**, 046607 (2007).
[25] S. Taravati, N. Chamanara, and C. Caloz, Phys. Rev. B **96**, 165144 (2017).
[26] M. Blaauboer, A. G. Kofman, A. E. Kozhekin, G. Kurizki, D. Lenstra, and A. Lodder, Phys. Rev. A **57**, 4905 (1998).

[27] See Supplemental Material at http://link.aps.org/supplemental/10.1103/PhysRevLett.123.206101 for details of numerical and analytical calculations, further verification via finite-element simulations and modelling of adiabatic graphene modulation, which includes Refs. [28–30].
[28] P. A. D. Gonçalves and N. M. Peres, *An Introduction to Graphene Plasmonics* (World Scientific, Singapore, 2016).
[29] E. S. Cassedy, Proc. Inst. Electr. Eng. **112**, 269 (1965).
[30] T. Stauber, N. M. R. Peres, and F. Guinea, Phys. Rev. B **76**, 205423 (2007).
[31] J. N. Winn, S. Fan, J. D. Joannopoulos, and E. P. Ippen, Phys. Rev. B **59**, 1551 (1999).
[32] D. Correas-Serrano, J. Gomez-Diaz, D. Sounas, Y. Hadad, A. Alvarez-Melcon, and A. Alù, IEEE Antennas Wireless Propag. Lett. **15**, 1529 (2015).
[33] T. Dinc, M. Tymchenko, A. Nagulu, D. Sounas, A. Alu, and H. Krishnaswamy, Nat. Commun. **8**, 795 (2017).
[34] K. Novoselov, A. Mishchenko, A. Carvalho, and A. C. Neto, Science **353**, aac9439 (2016).
[35] D. Basov, M. Fogler, and F. G. De Abajo, Science **354**, aag1992 (2016).
[36] F. H. Koppens, D. E. Chang, and F. J. García de Abajo, Nano Lett. **11**, 3370 (2011).
[37] A. Y. Nikitin, F. Guinea, F. J. Garcia-Vidal, and L. Martin-Moreno, Phys. Rev. B **84**, 195446 (2011).
[38] A. Grigorenko, M. Polini, and K. Novoselov, Nat. Photonics **6**, 749 (2012).
[39] L. Ju, B. Geng, J. Horng, C. Girit, M. Martin, Z. Hao, H. A. Bechtel, X. Liang, A. Zettl, Y. R. Shen *et al.*, Nat. Nanotechnol. **6**, 630 (2011).
[40] A. Vakil and N. Engheta, Science **332**, 1291 (2011).
[41] T. M. Slipchenko, M. Nesterov, L. Martin-Moreno, and A. Y. Nikitin, J. Opt. **15**, 114008 (2013).
[42] P. A. Huidobro, M. Kraft, S. A. Maier, and J. B. Pendry, ACS Nano **10**, 5499 (2016).
[43] J.-M. Poumirol, P. Q. Liu, T. M. Slipchenko, A. Y. Nikitin, L. Martin-Moreno, J. Faist, and A. B. Kuzmenko, Nat. Commun. **8**, 14626 (2017).
[44] C.-F. Chen, C.-H. Park, B. W. Boudouris, J. Horng, B. Geng, C. Girit, A. Zettl, M. F. Crommie, R. A. Segalman, S. G. Louie *et al.*, Nature (London) **471**, 617 (2011).
[45] D. K. Efetov and P. Kim, Phys. Rev. Lett. **105**, 256805 (2010).
[46] W. Li, B. Chen, C. Meng, W. Fang, Y. Xiao, X. Li, Z. Hu, Y. Xu, L. Tong, H. Wang *et al.*, Nano Lett. **14**, 955 (2014).
[47] A. C. Tasolamprou, A. D. Koulouklidis, C. Daskalaki, C. P. Mavidis, G. Kenanakis, G. Deligeorgis, Z. Viskadourakis, P. Kuzhir, S. Tzortzakis, M. Kafesaki *et al.*, ACS Photonics **6**, 720 (2019).
[48] L. Banszerus, M. Schmitz, S. Engels, J. Dauber, M. Oellers, F. Haupt, K. Watanabe, T. Taniguchi, B. Beschoten, and C. Stampfer, Sci. Adv. **1**, e1500222 (2015).
[49] D. A. Iranzo, S. Nanot, E. J. Dias, I. Epstein, C. Peng, D. K. Efetov, M. B. Lundeberg, R. Parret, J. Osmond, J.-Y. Hong *et al.*, Science **360**, 291 (2018).
[50] P. Alonso-González, A. Y. Nikitin, Y. Gao, A. Woessner, M. B. Lundeberg, A. Principi, N. Forcellini, W. Yan, S. Vélez, A. J. Huber *et al.*, Nat. Nanotechnol. **12**, 31 (2017).
[51] T. A. Morgado and M. G. Silveirinha, Phys. Rev. Lett. **119**, 133901 (2017).
[52] T. Wenger, G. Viola, J. Kinaret, M. Fogelström, and P. Tassin, Phys. Rev. B **97**, 085419 (2018).
[53] N. Ghafarian, H. Majedi, and S. Safavi-Naeini, IEEE J. Sel. Top. Quantum Electron. **23**, 179 (2016).
[54] J. Wilson, F. Santosa, M. Min, and T. Low, Phys. Rev. B **98**, 081411(R) (2018).
[55] Z. Sun, D. N. Basov, and M. M. Fogler, Phys. Rev. Lett. **117**, 076805 (2016).
[56] I. Kaminer, Y. T. Katan, H. Buljan, Y. Shen, O. Ilic, J. J. López, L. J. Wong, J. D. Joannopoulos, and M. Soljačić, Nat. Commun. **7**, ncomms11880 (2016).
[57] P. Knight and A. Miller, *Optical Solitons: Theory and Experiment* (Cambridge University Press, Cambridge, England, 1992), Vol. 10.

Supplementary Material for "Broadband Nonreciprocal Amplification in Luminal Metamaterials"

E. Galiffi, P. A. Huidobro and J. B. Pendry

October 16, 2019

Contents

1 Analytical Model

Consider a space-time dependent profile of the relative permittivity in a dispersionless medium:

$$\varepsilon = 1 + 2\alpha\cos(gx - \Omega t),$$

which moves with a phase velocity $c_p = \Omega/g$. Maxwell's equations in the medium read:

$$\nabla \times \mathbf{E} = -\frac{\partial \mathbf{B}}{\partial t} \qquad\qquad \nabla \times \mathbf{H} = \frac{\partial \mathbf{D}}{\partial t} \tag{1}$$

and taking the scalar product of these two expressions with $\mathbf{H}$ and $\mathbf{E}$ respectively, we get:

$$\mathbf{H} \cdot (\nabla \times \mathbf{E}) = -\mathbf{H} \cdot \frac{\partial \mathbf{B}}{\partial t} \qquad\qquad \mathbf{E} \cdot (\nabla \times \mathbf{H}) = \mathbf{E} \cdot \frac{\partial \mathbf{D}}{\partial t} \tag{2}$$

The difference between the last two equations gives:

$$\mathbf{H} \cdot (\nabla \times \mathbf{E}) - \mathbf{E} \cdot (\nabla \times \mathbf{H}) \equiv \nabla \cdot (\mathbf{E} \times \mathbf{H}) = -\mathbf{H} \cdot \frac{\partial \mathbf{B}}{\partial t} - \mathbf{E} \cdot \frac{\partial \mathbf{D}}{\partial t} \tag{3}$$

$$= -\frac{\mu_0}{2}\frac{\partial H^2}{\partial t} - \frac{\varepsilon\varepsilon_0}{2}\frac{\partial E^2}{\partial t} - \varepsilon_0 E^2 \frac{\partial \varepsilon}{\partial t} \tag{4}$$

Thus, the rate of change of the energy density in the fields is given by:

$$\frac{\partial U}{\partial t} = \frac{\mu_0}{2}\frac{\partial H^2}{\partial t} + \frac{\varepsilon\varepsilon_0}{2}\frac{\partial E^2}{\partial t} = -\varepsilon^{-1}\frac{\partial \varepsilon}{\partial t}U - \nabla \cdot (\mathbf{E} \times \mathbf{H}), \tag{5}$$

where, since the modulation can only pump energy into the electric field, we assumed that the electric contribution to the energy density $\frac{\varepsilon_0\varepsilon}{2}E^2 = U - \frac{\mu_0}{2}H^2 \simeq U$ dominates over the magnetic one. In one dimension, the latter is simply $\frac{\partial P}{\partial x}$, where P is the Poynting vector along the axis of propagation (i.e. x).

We now change variables $(x, t) \to (x - c_p t, t) = (X, t)$, effectively boosting our coordinates to the comoving frame. In this frame, the time derivative $\frac{\partial}{\partial t}$ must be substituted by the comoving derivative $\frac{d}{dt} = \frac{\partial}{\partial t} + c_p\frac{\partial}{\partial x}$, so that the energy density effectively takes on an advective term $c_p\frac{\partial U}{\partial x}$ from the Poynting flux acquired as a result of the boost, and Eq.5 becomes:

$$\frac{dU}{dt} = -\varepsilon^{-1}\frac{\partial \varepsilon}{\partial t}U - \frac{\partial P}{\partial x} - c_p\frac{\partial U}{\partial x} \tag{6}$$

At a first approximation, we ignore the Poynting contribution, so that we are left with:

$$\frac{dU}{dt} \simeq -\varepsilon^{-1}\frac{\partial \varepsilon}{\partial t}U \simeq -2\alpha\Omega\sin(gX)U \tag{7}$$

This is exact at the gain- and loss-points, as the second and third term in Eq. 6 cancel one another since the modulation amplitude vanishes there. Integrating the latter gives us the zero-order solution:

$$U(X,t) = e^{-2\alpha\Omega t \sin(gX)}, \tag{8}$$

where we took $U(t=0) = 1$.

We can get a correction to the above expression by recognising that the Poynting vector is given by the product of the local phase velocity $c(X,t) = \varepsilon^{-1/2} c_p$ with the local energy density $U(X,t)$. Plugging our zero-order solution for $U(X,t)$ into Eq. 6 yields:

$$\begin{aligned}
\frac{dU}{dt} &= -\varepsilon^{-1}\frac{\partial \varepsilon}{\partial t}U - c_p \frac{\partial}{\partial x}[(\varepsilon^{-1/2}(X,t) - 1)U(X,t)] && (9)\\
&\simeq -\varepsilon^{-1}\frac{\partial \varepsilon}{\partial t}U - c_p(\varepsilon^{-1/2} - 1)\frac{\partial U}{\partial x} && (10)\\
&\simeq [-2\alpha\Omega \sin(gX) - 2\alpha^2 c_p \Omega g t \cos^2(gX))]U && (11)
\end{aligned}$$

Finally, solving the latter (note: $c_p = \Omega/g$):

$$U(X,t) = e^{-2\alpha\Omega t \sin(gX) - \alpha^2\Omega^2 t^2 \cos^2(gX)} \tag{12}$$

Note that the Poynting contribution vanishes at the gain and loss points, indicating that the previous solution is indeed exact there.

2 Floquet-Bloch Theory: modulated dielectric

Here we present the Floquet-Bloch solution of the scattering problem through a finite space-time slab. Consider a space-time modulated dielectric with permittivity $\varepsilon = 1 + 2\alpha\cos(gx - \Omega t)$. We assume a solution of the form $\mathbf{E} = E_z\mathbf{z}$, $\mathbf{H} = H_x\mathbf{x} + H_y\mathbf{y}$, where

$$E_z = \sum_n E_n e^{i[(k+ng)x-(\omega+n\Omega)t]}, \quad H_y = \sum_n H_{y,n} e^{i[(k+ng)x-(\omega+n\Omega)t]}, \quad H_x = \sum_n H_{x,n} e^{i[(k+ng)x-(\omega+n\Omega)t]} \tag{13}$$

Plugging these into Maxwell's Equations, we retrieve an eigenvalue equation for k:

$$kE_n = -\sum_{n'} ng\delta_{n,n'}E_{n'} - \mu_0\sum_{n'}(\omega + n\Omega)\delta_{n,n'}H_{y,n'} \tag{14}$$

$$kH_{y,n} = -\sum_{n'} ng\delta_{n,n'}H_{y,n'} - \varepsilon_0\sum_{n'}\{(\omega + n\Omega)[\delta_{n,n'} + \alpha(\delta_{n+1,n'} + \delta_{n-1,n'})] + \Omega\alpha(\delta_{n+1,n'} - \delta_{n-1,n'})]\}E_{n'} \tag{15}$$

which can be written, in matrix form, as:

$$k\begin{pmatrix}\mathbf{E}\\ \mathbf{H}\end{pmatrix} = \begin{pmatrix}\mathbf{M}^{EE} & \mathbf{M}^{EH}\\ \mathbf{M}^{HE} & \mathbf{M}^{HH}\end{pmatrix}\begin{pmatrix}\mathbf{E}\\ \mathbf{H}\end{pmatrix} \tag{16}$$

For $\alpha = 0$, the eigenvalues

$$k_{vn}^{\pm} = -ng \pm \sqrt{c_0^{-2}(\omega + n\Omega)^2} \tag{17}$$

and eigenvectors

$$\mathbf{v}_\mathbf{n}^{\pm} = \begin{pmatrix}1\\ (ng + k_{vn}^{\pm})/\mu_0(\omega + n\Omega)\end{pmatrix} \tag{18}$$

may be calculated analytically. Calculating the sign of the resulting group velocity enables the determination of left- and right-propagating waves in the vacuum regions.

Subsequently, we can write the fields in the two regions outside of the luminal metamaterial as superpositions of the vacuum eigenvectors:

$$\begin{pmatrix}\mathbf{E}_{\mathbf{v,z}}^{(1)}\\ \mathbf{H}_{\mathbf{v,y}}^{(1)}\end{pmatrix} = \mathbf{M}^{\mathbf{vinc}}\mathbf{e}_{\mathbf{vinc}}^{(1)} + \mathbf{M}^{\mathbf{vref}}\mathbf{e}_{\mathbf{vref}}^{(1)} \qquad \begin{pmatrix}\mathbf{E}_{\mathbf{v,z}}^{(2)}\\ \mathbf{H}_{\mathbf{v,y}}^{(2)}\end{pmatrix} = \mathbf{M}^{\mathbf{vinc}}\mathbf{e}_{\mathbf{vtra}}^{(2)} \tag{19}$$

and inside the metamaterial:

$$\begin{pmatrix}\mathbf{E}_{\mathbf{m,z}}^{(1)}\\ \mathbf{H}_{\mathbf{m,y}}^{(1)}\end{pmatrix} = \mathbf{M}^{\mathbf{m}}\mathbf{e}_{\mathbf{m}} \qquad \begin{pmatrix}\mathbf{E}_{\mathbf{m,z}}^{(2)}\\ \mathbf{H}_{\mathbf{m,y}}^{(2)}\end{pmatrix} = \mathbf{M}^{\mathbf{m}}\mathbf{P}\mathbf{e}_{\mathbf{m}} \tag{20}$$

where $\mathbf{M}^{\mathbf{vinc}}$ and $\mathbf{M}^{\mathbf{vref}}$ are rectangular matrices containing the right- and left-propagating eigenvectors respectively, $\mathbf{M}^{\mathbf{m}}$ is a square matrix containing all eigenvectors inside of the metamaterial,

and $\mathbf{P}$ is a diagonal matrix $P_{mn} = \exp(ik_m d)\delta_{mn}$ which propagates each eigenvector from the left to the right interface. Applying the continuity of E_z and H_y at the two interfaces, we arrive at a matrix equation:

$$\begin{pmatrix} \mathbf{A} & \mathbf{B} \end{pmatrix} \begin{pmatrix} \mathbf{e^{(2)}_{vtr}} \\ \mathbf{e^{(2)}_{vref}} \end{pmatrix} = \begin{pmatrix} \mathbf{M^{vinc}} & 0 \end{pmatrix} \begin{pmatrix} \mathbf{e^{(1)}_{vinc}} \\ 0 \end{pmatrix} \tag{21}$$

where:

$$\mathbf{A} = \mathbf{M^{m}}(\mathbf{M}^{m}\mathbf{P})^{-1}\mathbf{M^{vinc}} \qquad\qquad \mathbf{B} = -\mathbf{M^{mvref}} \tag{22}$$

are rectangular matrices, such that their concatenation is square, so that the transmitted and reflected amplitudes can be readily calculated by inverting Eq. 21.

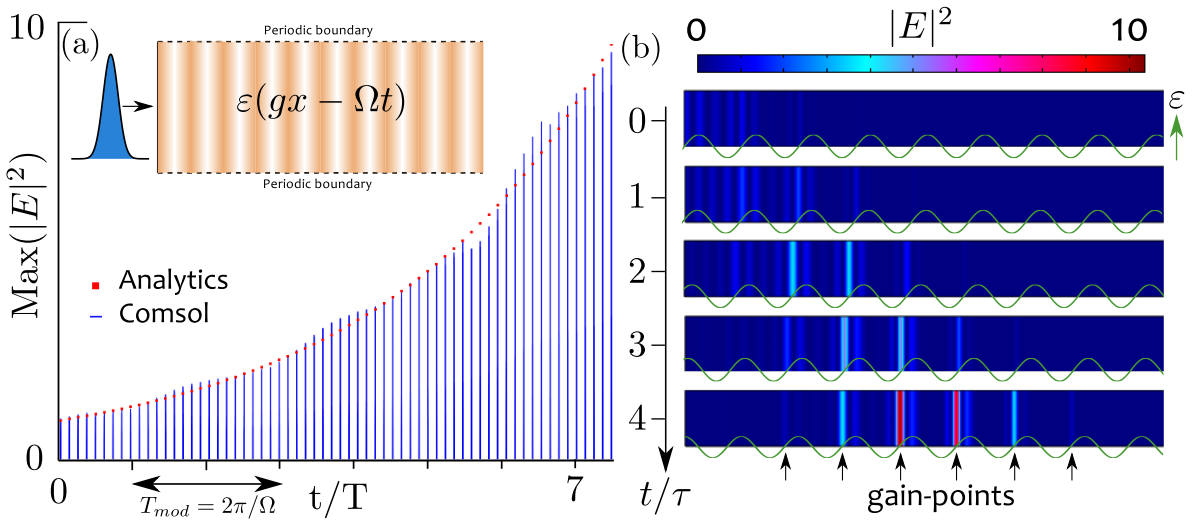

Figure 1: (a) Maximum electric field intensity of a pulse propagating through a luminal metamaterial as calculated in COMSOL (blue bars), and predicted by our analytic model (red dots). The inset shows the physical setup. (b) Field plot of the electric field intensity along the slab as time increases (rows). The green curves represent the phase of the spatial modulation profile at the different times, demonstrating that amplification takes place at the gain points.

3 Finite-Element Time-Domain Simulations

Here we provide the results of fully numerical simulations obtained with the numerical package COMSOL Multiphysics. The system is depicted in Fig. 1a (inset): a gaussian pulse,

$$E(x,t) = cos(\omega_0 t - k_0 x) e^{-(t-t_0)^2/\Delta t^2}, \tag{23}$$

with carrier wavelength $\omega_0 \approx 1.88$ rad/fs (corresponding to $k_0 = 6.28$ rad/μm) and width $\Delta t = 13$ fs is injected from the left side of a slab of width L_g (with periodic boundary conditions above and below), subject to a permittivity modulation $\delta\varepsilon = 2\alpha\cos(gx - \Omega t)$, where $\alpha = 0.05$, $g \approx 3.14$ rad/μm, $\Omega \approx 0.942$ rad/fs. The spatial length of the grating is $L_g = 2$ μm, the carrier wavelength $\lambda_0 = 1$ μm.

After a time delay $t_0 = 35$ fs, we measure the peak of the electric field intensity $\max|E|^2$ in the pulse as it evolves over time. In Fig. 1a we compare its exponential increase with that predicted by our analytic model: $|E|^2 \propto \exp(2\alpha\Omega t)$ demonstrating excellent matching between the two.

Fig. 1b shows the intensity profile along the slab at subsequent time instants (corresponding to the different rows). The green sinusoids depict the phase of the modulation profile at the different times, highlighting the fact that the amplification mechanism follows closely the explanation given in the main manuscript. We point out that the additional wiggles are due to the use of a real carrier wave, as opposed to the complex phasor used in the analytic and Floquet-Bloch calculations.

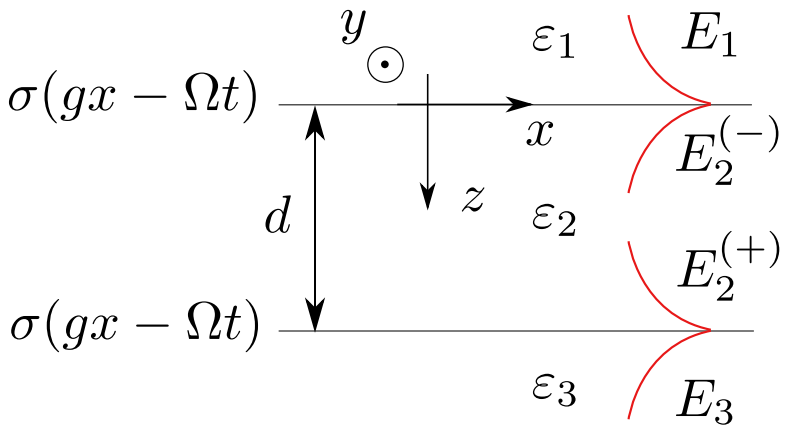

Figure 2: Setup for modulated double-layer graphene (DLG). The top surface sits at $z = 0$, whereas the bottom one sits at $z = d$.

4 Floquet-Bloch Theory: modulated double-layer graphene

Here we consider surface plasmons on spatiotemporally modulated double-layer graphene (DLG), assuming that the conductivity profile is the same on both graphene layers. The setup is shown in Fig. 2. We solve Maxwell's Equations (MEs) in each domain, and introduce an auxiliary equation for the surface current J, which, coupled to the boundary conditions, introduces the coupling between different Floquet-Bloch modes of the structure induced by the modulation.

4.1 Uniformly doped Double Layer Graphene

On uniformly doped DLG, the p-polarised plasmon fields read [1]:

$$\mathbf{E_j} = (E_{j,x}\hat{\mathbf{x}} + E_{j,z}\hat{\mathbf{z}})e^{-\kappa_j|z|}e^{i(kx-\omega t)} \tag{24}$$

$$\mathbf{B_j} = B_{j,y}\hat{\mathbf{y}}e^{-\kappa_j|z|}e^{i(kx-\omega t)} \tag{25}$$

for $j = 1, 3$ and:

$$\mathbf{E_2} = \left[(E_{2,x}^{(+)}\hat{\mathbf{x}} + E_{2,z}^{(+)}\hat{\mathbf{z}})e^{\kappa_2|z|} + (E_{2,x}^{(-)}\hat{\mathbf{x}} + E_{2,z}^{(-)}\hat{\mathbf{z}})e^{-\kappa_2|z|}\right]e^{i(kx-\omega t)} \tag{26}$$

$$\mathbf{B_2} = \left[B_{2,y}^{(+)}\hat{\mathbf{y}}e^{\kappa_2|z|} + B_{2,y}^{(-)}\hat{\mathbf{y}}e^{-\kappa_2|z|}\right]e^{i(kx-\omega t)}, \tag{27}$$

where k is the in-plane wavevector, ω is the plasmon frequency and κ_j is the out-of-plane decay constant in the j^{th} domain. The relations between the magnetic field and electric field amplitudes, which are derived from MEs in the three domains, read [1]:

$$B_{j,y} = -\frac{\omega\varepsilon_j}{c^2 k}E_{j,z} \qquad\qquad B_{j,y} = -i\,\mathrm{sgn}\,z\frac{\omega\varepsilon_j}{c^2\kappa_j}E_{j,x} \tag{28}$$

for $j = 1, 3$ and:

$$B_{2,y}^{(+)} = -\frac{\omega\varepsilon_2}{c^2 k} E_{2,z}^{(+)} \qquad B_{2,y}^{(+)} = i\frac{\omega\varepsilon_2}{c^2\kappa_2} E_{2,x}^{(+)} \tag{29}$$

$$B_{2,y}^{(-)} = -\frac{\omega\varepsilon_2}{c^2 k} E_{2,z}^{(-)} \qquad B_{2,y}^{(-)} = -i\frac{\omega\varepsilon_2}{c^2\kappa_2} E_{2,x}^{(-)} \tag{30}$$

Furthermore, MEs give us: $\kappa_j = \sqrt{k^2 - \varepsilon_j\omega^2/c^2}$

4.2 Modulated DLG

In order to account for the travelling-wave modulation, we generalise this ansatz as customary [2]:

$$\mathbf{E_j} = e^{i(kx-\omega t)} \sum_{n=-N_g}^{N_g} (E_{j,x,n}\hat{\mathbf{x}} + E_{j,z,n}\hat{\mathbf{z}}) e^{-\kappa_{j,n}|z|} e^{in(gx-\Omega t)} \tag{31}$$

$$\mathbf{B_j} = e^{i(kx-\omega t)} \sum_{n=-N_g}^{N_g} B_{j,y,n}\hat{\mathbf{y}} e^{-\kappa_{j,n}|z|} e^{in(gx-\Omega t)} \tag{32}$$

for $j = 1, 3$, where we defined:

$$\kappa_{j,n} = \sqrt{(k+ng)^2 - \varepsilon_j(\omega+n\Omega)^2/c^2} \tag{33}$$

Similarly, for $j = 2$ we have:

$$\mathbf{E_2} = e^{i(kx-\omega t)} \sum_n \left[(E_{2,x,n}^{(+)}\hat{\mathbf{x}} + E_{2,z,n}^{(+)}\hat{\mathbf{z}}) e^{\kappa_{2,n}z} + (E_{2,x,n}^{(-)}\hat{\mathbf{x}} + E_{2,z,n}^{(-)}\hat{\mathbf{z}}) e^{-\kappa_{2,n}z} \right] e^{in(gx-\Omega t)} \tag{34}$$

$$\mathbf{B_2} = e^{i(kx-\omega t)} \sum_n \left[B_{2,y,n}^{(+)}\hat{\mathbf{y}} e^{\kappa_{2,n}z} + B_{2,y,n}^{(-)}\hat{\mathbf{y}} e^{-\kappa_{2,n}z} \right] e^{in(gx-\Omega t)} \tag{35}$$

In the absence of a modulation in the conductivity of graphene, the ansatz above would simply return a separate solution for each individual Floquet-Bloch (FB) mode. However, care must be taken that $\Re[\kappa_{j,n}] > 0\ \forall n$, or we would have solutions which grow exponentially away from the graphene. We can then generalise the previous relations between the amplitudes as:

$$B_{j,y,n} = -\frac{(\omega+n\Omega)\varepsilon_j}{c^2(k+ng)} E_{j,z,n} \qquad B_{j,y,n} = -i\,\mathrm{sgn}\,z\frac{(\omega+n\Omega)\varepsilon_j}{c^2\kappa_{j,n}} E_{j,x,n} \tag{36}$$

for $j = 1$ ($\mathrm{sgn}\,(z) < 0$), 3 ($\mathrm{sgn}\,(z) > 0$) and:

$$B^{(+)}_{2,y,n} = -\frac{(\omega + n\Omega)\varepsilon_2}{c^2(k+ng)} E^{(+)}_{2,z,n} \qquad B^{(+)}_{2,y,n} = i\frac{(\omega + n\Omega)\varepsilon_2}{c^2\kappa_{2,n}} E^{(+)}_{2,x,n} \tag{37}$$

$$B^{(-)}_{2,y,n} = -\frac{(\omega + n\Omega)\varepsilon_2}{c^2(k+ng)} E^{(-)}_{2,z,n} \qquad B^{(-)}_{2,y,n} = -i\frac{(\omega + n\Omega)\varepsilon_2}{c^2\kappa_{2,n}} E^{(-)}_{2,x,n} \tag{38}$$

$$\tag{39}$$

We thus have $12(2N_g + 1)$ unknowns: $6(2N_g + 1)$ coefficients for the fields in the $j = 2$ region, and $3(2N_g + 1)$ coefficients for each of the $j = 1, 3$ regions.

In order to solve for the fields, we already have $8(2N_g + 1)$ equations for the amplitudes: $4(2N_g + 1)$ equations relating the field amplitudes in the $j = 2$ region, and $2(2N_g + 1)$ for each of the $j = 1, 3$ regions. The $4(2N_g + 1)$ missing equations are obtained by imposing continuity of the in-plane electric fields E_x at $z = 0$, and $z = d$:

$$E^{(+)}_{2,x,n} + E^{(-)}_{2,x,n} = E_{1,x,n} \tag{40}$$

$$E^{(+)}_{2,x,n} e^{\kappa_{2,n} d} + E^{(-)}_{2,x,n} e^{-\kappa_{3,n} d} = E_{3,x,n} e^{-\kappa_{3,n} d} \tag{41}$$

and by imposing discontinuity of the magnetic field B_y/μ_0 by the surface current $J(x, t)$:

$$e^{i(kx-\omega t)} \sum_n \left[B_{1,y,n} - (B^{(+)}_{2,y,n} + B^{(-)}_{2,y,n}) \right] e^{in(gx-\Omega t)} = \mu_0 J_0(x, t) \tag{42}$$

$$e^{i(kx-\omega t)} \sum_n \left[B^{(+)}_{2,y,n} e^{\kappa_{2,n} d} + B^{(-)}_{2,y,n} e^{-\kappa_{2,n} d} - B_{3,y,n} e^{-\kappa_{3,n} d} \right] e^{in(gx-\Omega t)} = \mu_0 J_d(x, t) \tag{43}$$

where we denoted by J_0 and J_d the surface current at the top (z=0) and bottom (z=d) graphene sheets respectively. In order to account for dispersion in the response of graphene, however, we introduce the surface current via an auxiliary equation, obtained from a semiclassical treatment of the graphene optical conductivity (see Sec. 5), which gives:

$$J_n = \frac{e^2 \epsilon_{F,0}}{\pi \hbar^2} \frac{[E_n + \alpha(E_{n+1} + E_{n-1})]}{\gamma - i\omega + n\Omega} \tag{44}$$

Hence, the space-time modulation introduces a frequency-wavevector coupling between Fourier amplitudes of the electric and magnetic field.

4.3 Derivation of the eigenvalue problem for ω

For simplicity, we shall also assume that we are in a symmetric environment, with equal dielectrics on either sides, so that $\varepsilon_1 = \varepsilon_2 = \varepsilon_3 = \varepsilon$, $\kappa_{1,n} = \kappa_{2,n} = \kappa_{3,n} = \kappa_n$ and $J_0 = J_d$. The system then has reflection symmetry with respect to the $z = d/2$ axis. This halves the number of equations that we have to solve, since, for the acoustic mode, we have [1]:

$$E_x(z = d/2 - \Delta) = -E_x(z = d/2 + \Delta) \tag{45}$$
$$E_z(z = d/2 - \Delta) = E_z(z = d/2 + \Delta) \tag{46}$$
$$B_y(z = d/2 - \Delta) = B_y(z = d/2 + \Delta) \tag{47}$$

We choose to match the fields at $z = 0$. Inserting our expression for J_n in the appropriate boundary condition (Eq. 42):

$$\left[B_{1,y,n} - (B^{(+)}_{2,y,n} + B^{(-)}_{2,y,n})\right] = \frac{\mu_0 e^2}{\pi\hbar^2}\frac{1}{[\gamma - i(\omega + n\Omega)]}[\epsilon_F E_{1,x,n} + \alpha(E_{1,x,n-1} + E_{1,x,n+1})] \tag{48}$$
$$E^{(+)}_{2,x,n} + E^{(-)}_{2,x,n} = E_{1,x,n} \tag{49}$$

By symmetry of the acoustic mode: $B^{(-)}_{2,y,n} = e^{\kappa_n d}B^{(+)}_{2,y,n}$. Substituting the magnetic field for the electric field in Eq. 49 by using:

$$E_{1,x,n} = -i\frac{c^2\kappa_n}{(\omega + n\Omega)\varepsilon}B_{1,y,n} \quad E^{(+)}_{2,x,n} = -i\frac{c^2\kappa_n}{(\omega + n\Omega)\varepsilon}B^{(+)}_{2,y,n} \quad E^{(-)}_{2,x,n} = +i\frac{c^2\kappa_n}{(\omega + n\Omega)\varepsilon}B^{(-)}_{2,y,n} \tag{50}$$

and dividing through by the common prefactors, Eq. 49 becomes:

$$B^{(+)}_{2,y,n} - B^{(-)}_{2,y,n} = B_{1,y,n} \tag{51}$$

And exploiting the symmetry of the fields:

$$(1 - e^{\kappa_n d})B^{(+)}_{2,y,n} = B_{1,y,n} \tag{52}$$
$$B^{(+)}_{2,y,n} = \frac{1}{1 - e^{\kappa_n d}}B_{1,y,n} \tag{53}$$

$$B_{1,y,n} - (B^{(+)}_{2,y,n} + B^{(-)}_{2,y,n}) = B_{1,y,n} - (1 + e^{\kappa_n d})B^{(+)}_{2,y,n} \tag{54}$$
$$= \left(1 - \frac{1 + e^{\kappa_n d}}{1 - e^{\kappa_n d}}\right)B_{1,y,n} \tag{55}$$

Hence, substituting into the first boundary condition:

$$\left[B_{1,y,n} - (B^{(+)}_{2,y,n} + B^{(-)}_{2,y,n})\right] = \frac{\mu_0 e^2}{\pi\hbar^2}\frac{\epsilon_{F,0}}{\gamma - i(\omega + n\Omega)}[E_{1,x,n} + \alpha(E_{1,x,n-1} + E_{1,x,n+1})] \tag{56}$$
$$\left(1 - \frac{1 + e^{\kappa d}}{1 - e^{\kappa_n d}}\right)B_{1,y,n} = \frac{1}{\gamma - i(\omega + n\Omega)}\sum_{n'}\Lambda_{n,n'}E_{n'} \tag{57}$$
$$[\gamma - i(\omega + n\Omega)]B_{1,y,n} = \left(1 - \frac{1 + e^{\kappa_n d}}{1 - e^{\kappa_n d}}\right)^{-1}\sum_{n'}\Lambda_{n,n'}E_{n'} \tag{58}$$
$$\omega B_{1,y,n} = -(n\Omega + i\gamma)B_{1,y,n} + i\left(1 - \frac{1 + e^{\kappa_n d}}{1 - e^{\kappa_n d}}\right)^{-1}\sum_{n'}\Lambda_{n,n'}E_{n'} \tag{59}$$

where we defined: $\Lambda_{n,n'} = \frac{\mu_0 e^2 \epsilon_{F,0}}{\pi\hbar^2}[\delta_{n,n'} + \alpha(\delta_{n,n'-1} + \delta_{n,n'+1})]$. In order to write an eigenvalue problem for our system, we solve this simultaneously with the first of Eqs. 50:

$$(\omega + n\Omega)E_{1,x,n} = -\frac{ic^2\kappa_n}{\varepsilon_1}B_{1,y,n} \tag{60}$$

$$\omega E_{1,x,n} = -n\Omega E_{1,x,n} - \frac{ic^2\kappa_n}{\varepsilon}B_{1,y,n} \tag{61}$$

We shall hereafter omit the subscripts indicating the domain and dimensional component of the field coefficients, denoting $E_{1,x,n} \to E_n$ and $B_{1,x,n} \to B_n$. We can then use the quasistatic approximation: $\kappa_n = \sqrt{(k+ng)^2 - \epsilon(\omega + n\Omega)^2/c^2} \simeq \sqrt{(k+ng)^2}$, since $k \ll k_0$ $k_0 \ll k$, $g \ll k$ and $\Omega \ll \omega$. The full eigenvalue problem for ω thus reads:

$$\omega E_n = -n\Omega E_n - \frac{ic^2\sqrt{(k+ng)^2}}{\varepsilon}B_{n'} \tag{62}$$

$$\omega B_n = \sum_{n'}\Bigg\{\Bigg[i\left(1 + \frac{e^{\sqrt{(k+ng)^2}d}+1}{e^{\sqrt{(k+ng)^2}d}-1}\right)^{-1}\Lambda_{n,n'}E_{n'} \tag{63}$$

$$- (n\Omega + i\gamma)B_n \tag{64}$$

The inverse of the term in big round brackets can be written as $\frac{1}{2}(1 - e^{-\sqrt{(k+ng)^2}d})$, so that the equations read, in matrix form:

$$\omega\begin{pmatrix}\mathbf{E}\\ \mathbf{B}\end{pmatrix} = \begin{pmatrix}\boldsymbol{M^{EE}} & \boldsymbol{M^{EB}}\\ \boldsymbol{M^{BE}} & \boldsymbol{M^{BB}}\end{pmatrix}\begin{pmatrix}\mathbf{E}\\ \mathbf{B}\end{pmatrix} = \boldsymbol{\Theta}\begin{pmatrix}\mathbf{E}\\ \mathbf{B}\end{pmatrix} \tag{65}$$

with:

$$M^{EE}_{n,n'} = -n'\Omega\delta_{n,n'} \qquad M^{EB}_{n,n'} = -\frac{ic^2\sqrt{(k+n'g)^2}}{\varepsilon}\delta_{n,n'} \tag{66}$$

$$M^{BE}_{n,n'} = \frac{i}{2}(1 - e^{-\sqrt{(k+ng)^2}d})\Lambda_{n,n'} \qquad M^{BB}_{n,n'} = -(n'\Omega + i\gamma)\delta_{n,n'} \tag{67}$$

For convenience, we can define dimensionless variables such that the plasmon velocity at $k = 0$:

$$\lim_{k\to 0} v_p(k) = \sqrt{\frac{e^2\epsilon_F d}{2\varepsilon_0\varepsilon\pi\hbar^2}} = c_p \tag{68}$$

takes the value 1, $k \to \hat{k} = kd$, $\omega \to \hat{\omega} = \omega d/c_p(k=0)$. An alternative method to account for dispersion is to expand the exponential in powers of $(k+ng)$, truncate the series and solve a nonlinear eigenvalue problem. However, the choice of solutions with the right behaviour at $z \to \pm\infty$ is non-trivial in this case, and it would realistically only account for dispersion to first or second order. On the contrary, solving the eigenvalue problem for ω, and subsequently performing the scattering problem in the time domain allows us to retain the full dispersion.

4.4 Unmodulated case

In the unmodulated case $\alpha = 0$, and $\hat{\Lambda}_{n,n'} = \delta_{n,n'}$ so the eigenvalues:

$$\omega_{vn}^{\pm} = -\frac{i\gamma}{2} \pm \sqrt{\sqrt{(k+ng)^2}(1 - e^{-\sqrt{(k+ng)^2}}) - \frac{\gamma^2}{4}} \tag{69}$$

can be calculated analytically, (omitting the hats). Note that, due to the quasistatic approximation used $\kappa_n = \sqrt{(k+ng)^2 - \epsilon(\omega + n\Omega)^2} \simeq \sqrt{(k+ng)^2}$, this calculation cannot account for transient waves at the temporal boundaries. This is valid, since the modulation is adiabatic, and the effect of the sustained amplification dominates over any transient effects. From Eq. 69 we can calculate the group velocity:

$$\frac{\partial \omega_{vn}^{\pm}}{\partial k} = \mathrm{sgn}\,(k+ng)\frac{(1 - e^{-\sqrt{(k+ng)^2}} + \sqrt{(k+ng)^2}e^{-\sqrt{(k+ng)^2}})}{2(\omega_{vn}^{\pm} + n\Omega)} \tag{70}$$

whose real part gives us the direction of propagation, thus allowing us to distinguish between forward and backward-propagating waves. The normalised eigenvectors are:

$$v_n^{\pm} = \begin{pmatrix} E_n \\ B_n \end{pmatrix} = \begin{pmatrix} 1 \\ \frac{i(\omega_{vn}^{\pm} + n\Omega)}{\sqrt{(k+ng)^2}} \end{pmatrix} \Big/ \left[1 + \frac{|\omega_{vn}^{\pm} + n\Omega|^2}{(k+ng)^2}\right]^{1/2} \tag{71}$$

Finally, we point out that, for forward-travelling waves $\sim e^{-i\omega t}$ to decay over time, the eigenvalues ω must have a negative imaginary part, so that the effect of loss is to damp the waves as they propagates forward in time. By contrast, waves which are time-reversed as a result of the modulation need to have a positive imaginary part. Hence, once identified, we must take their complex conjugate.

4.5 Scattering Problem in the time domain

We now calculate the scattering across a temporal window, during which the travelling-wave modulation is applied, and calculate the transmitted and time-reversed waves. At times $t < 0$ the plasmon is propagating with frequency ω and wavevector k. As the doping modulation is switched on at $t = 0$, the system is periodic in space, so that its original quasi-momentum k is conserved. We can thus obtain the associated frequency eigenvalues, and propagate the solution up to time $t = T_f$, when it is switched off, and the pulse will consist of a forward-traveling wave, and a time-reversed one. The convenience of this approach is that the quasi-momentum k is a good quantum number, since the modulation is applied along an infinite graphene sheet. Hence, we can retain all the dispersion, without needing to solve a nonlinear eigenvalue problem as in an "on-shell" calculation for $k(\omega)$.

We first expand the solution at the inner sides of the two time-interfaces $t = 0^+$ and $t = T_f^-$ into a superposition of eigenmodes of the modulated graphene:

$$\begin{pmatrix} E_m^{(1)} \\ B_m^{(1)} \end{pmatrix} = \boldsymbol{M}^m \mathbf{e}^m \qquad\qquad \begin{pmatrix} E_m^{(2)} \\ B_m^{(2)} \end{pmatrix} = \boldsymbol{M}^m \boldsymbol{P} \mathbf{e}^m, \tag{72}$$

where $\mathbf{e_m}$ is a vector containing the amplitudes of each eigenvector contributing to the fields at the first temporal boundary, $\boldsymbol{M^m}$ is a $2(2N_g+1)(rows) \times 2(2N_g+1)(columns)$ matrix, which contains one eigenvector of the modulated system for each column, and $P_{jj} = e^{-i\omega_j T_f}$, ω_j is a diagonal matrix which contains the eigenvalues of the modulated system, propagating the eigenmodes from the first to the second temporal interface.

Before ($t = 0^-$) and after ($t = T_f^+$) switching on the modulation, the fields read:

$$\begin{pmatrix} E_v^{(1)} \\ B_v^{(1)} \end{pmatrix} = \boldsymbol{M}^{inc} \mathbf{e}^{inc} \qquad\qquad \begin{pmatrix} E_v^{(2)} \\ B_v^{(2)} \end{pmatrix} = \boldsymbol{M}^{inc} \mathbf{e}^{tra} + \boldsymbol{M}^{ref} \mathbf{e}^{ref}, \tag{73}$$

where $\boldsymbol{M^{inc}}$ and $\boldsymbol{M}^{ref}$ are $(2 \times (2N_g + 1))(rows) \times (2N_g + 1)(columns)$ matrices, whose columns contain the forward-propagating eigenvectors of the unmodulated system, and $\mathbf{e}^{inc}$ and $\mathbf{e}^{ref}$ contains their respective amplitudes.

In order to apply boundary conditions at $t = 0$ and $t = T_f$, respectively, we set:

$$\begin{pmatrix} E_m^{(1)} \\ B_m^{(1)} \end{pmatrix} = \boldsymbol{M}^m \mathbf{e}^m = \boldsymbol{M}^{inc} \mathbf{e}^{inc} = \begin{pmatrix} E_v^{(1)} \\ B_v^{(1)} \end{pmatrix} \tag{74}$$

$$\begin{pmatrix} E_m^{(2)} \\ B_m^{(2)} \end{pmatrix} = \boldsymbol{M}^m \boldsymbol{P} \mathbf{e}^m = \boldsymbol{M}^{inc} \mathbf{e}^{tra} + \boldsymbol{M}^{ref} \mathbf{e}^{ref} = \begin{pmatrix} E_v^{(2)} \\ B_v^{(2)} \end{pmatrix} \tag{75}$$

Multiplying the latter by $\boldsymbol{M}^m(\boldsymbol{M}^m \boldsymbol{P})^{-1}$ we obtain:

$$\boldsymbol{M}^m(\boldsymbol{M}^m \boldsymbol{P})^{-1}(\boldsymbol{M}^m \boldsymbol{P})\mathbf{e}^m = \boldsymbol{M}^m \mathbf{e}^m = [\boldsymbol{M}^m(\boldsymbol{M}^m \boldsymbol{P})^{-1}] \begin{pmatrix} \boldsymbol{M}^{inc} & \boldsymbol{M}^{ref} \end{pmatrix} \begin{pmatrix} \mathbf{e}^{tra} \\ \mathbf{e}^{ref} \end{pmatrix} = \boldsymbol{Q} \begin{pmatrix} \mathbf{e}^{tra} \\ \mathbf{e}^{ref} \end{pmatrix} \tag{76}$$

and substituting Eq.76 into Eq. 74:

$$\boldsymbol{Q} \begin{pmatrix} \mathbf{e}^{tra} \\ \mathbf{e}^{ref} \end{pmatrix} = \begin{pmatrix} \boldsymbol{M^{inc}} & 0 \end{pmatrix} \begin{pmatrix} \mathbf{e}^{inc} \\ 0 \end{pmatrix}, \tag{77}$$

which can be solved by direct inversion and substituted in the Fourier expansion of the fields.

5 Semiclassical theory of doping modulation

This calculation follows the argument in [1, 3], and assumes that the modulation is spatially and temporally adiabatic, compared to any electron relaxation processes. We start from the Boltzmann equation for the distribution $g_{\mathbf{k},t}$, which is the non-equilibrium contribution to the full distribution $f(\epsilon_{\mathbf{k}}) = f^0(\epsilon_k) + g_{\mathbf{k}}$:

$$-\frac{\partial f^0(\epsilon_{\mathbf{k}})}{\partial \epsilon_{\mathbf{k}}} e\mathbf{v}_{\mathbf{k}} \cdot \mathbf{E} = \frac{g_{\mathbf{k}}}{\tau_{\mathbf{k}}} + \mathbf{v}_{\mathbf{k}} \cdot \nabla_{\mathbf{r}} g_{\mathbf{k}} + \frac{\partial g_{\mathbf{k}}}{\partial t}, \tag{78}$$

$f^0(\epsilon_k)$ being the Fermi-Dirac distribution. The solution of the equation above is:

$$g_{\mathbf{k}} = -\frac{\partial f^0(\epsilon_{\mathbf{k}})}{\partial \epsilon_{\mathbf{k}}} \Phi_{\mathbf{q}}(\omega, k) e^{i(\mathbf{q}\cdot\mathbf{r} - \omega t)} \tag{79}$$

where:

$$\Phi_{\mathbf{q}}(\omega, q) = \frac{e\tau \mathbf{v}_{\mathbf{k}} \cdot \mathbf{E}}{1 - i\omega\tau + i\tau \mathbf{q} \cdot \mathbf{v}_{\mathbf{k}}} \tag{80}$$

Note that we are using q for the wavevector of the electromagnetic wave, and k for that of the electrons. In order to include the adiabatic spatiotemporal modulation of the graphene Fermi level $\epsilon_F(x,t) = \epsilon_{F,0}(1 + 2\alpha\cos(gx - \Omega t)$, we write:

$$f^m(\epsilon_{\mathbf{k}}, x, t) = \frac{1}{e^{(\epsilon_{\mathbf{k}} - \epsilon_F(x,t))/k_B T} + 1} \tag{81}$$

which is valid provided that $\Omega \ll \omega$, and $g \ll q$, so that we have:

$$\frac{\partial f^m}{\partial \epsilon_{\mathbf{k}}} = -\frac{1}{k_B T} \frac{e^{(\epsilon_{\mathbf{k}} - E_{F,0}(1+2\alpha\cos(gx-\Omega t))})T}{(e^{(\epsilon_{\mathbf{k}} - E_{F,0}(1+2\alpha\cos(gx-\Omega t))/k_B T} + 1)^2} \tag{82}$$

We neglect nonlocality effects, which are contained in the diffusive term $\mathbf{v}_{\mathbf{k}} \cdot \nabla_{\mathbf{r}} g_{\mathbf{k}}$ term of Eq. 78, and are not expected to modify qualitatively the physics described in this work. We thus get:

$$-\frac{\partial f^m(\epsilon_{\mathbf{k}}, x, t)}{\partial \epsilon_{\mathbf{k}}} e\mathbf{v}_{\mathbf{k}} \cdot \mathbf{E} = \frac{g_{\mathbf{k}}}{\tau_{\mathbf{k}}} + \frac{\partial g_{\mathbf{k}}}{\partial t} \tag{83}$$

We now multiply by the surface element $d^2\mathbf{k}$ and $e\mathbf{v}_{\mathbf{k}}$, and integrate over k-space, assuming that the collision rate $\gamma = 1/\tau$ is independent of $\mathbf{k}$, and using $\mathbf{v}_{\mathbf{k}} \cdot \mathbf{E} = v_F E_x \cos(\theta)$:

$$-e^2 \int d^2\mathbf{k} \frac{\partial f^m(\epsilon_{\mathbf{k}}, x, t)}{\partial \epsilon_{\mathbf{k}}} \mathbf{v}_{\mathbf{k}} (\mathbf{v}_{\mathbf{k}} \cdot \mathbf{E}) = (\gamma + \frac{\partial}{\partial t}) \int d^2\mathbf{k} e\mathbf{v}_{\mathbf{k}} g_{\mathbf{k}} \tag{84}$$

We can now use the fact that:

$$J_n = \frac{g_v g_s}{4\pi^2}\int d^2\mathbf{k} e\mathbf{v}_\mathbf{k} g_\mathbf{k} = \frac{2\cdot 2}{4\pi^2}\int d^2\mathbf{k} e\mathbf{v}_\mathbf{k} g_\mathbf{k} = \frac{1}{\pi^2}\int d^2\mathbf{k} e\mathbf{v}_\mathbf{k} g_\mathbf{k} \tag{85}$$

where g_v and g_s are the valley and spin degeneracies, both equal to 2, to re-write Eq. 83 as:

$$-e^2\int d^2\mathbf{k}\frac{\partial f^m(\epsilon_\mathbf{k},x,t)}{\partial\epsilon_\mathbf{k}}\mathbf{v}_\mathbf{k}(\mathbf{v}_\mathbf{k}\cdot\mathbf{E}) = \pi^2(\gamma+\frac{\partial}{\partial t})\mathbf{J} \tag{86}$$

To evaluate the LHS, we transform the integral to polar coordinates, and multiply both sides by $\hat{\mathbf{x}}$ in order to obtain J_x:

$$-e^2 v_F^2 E\int kdk\frac{\partial f^m(\epsilon_\mathbf{k},x,t)}{\partial\epsilon_\mathbf{k}}\int_0^{2\pi}\cos^2(\theta)d\theta = \pi^2(\gamma+\frac{\partial}{\partial t})J \tag{87}$$

Introducing the linear dispersion of Dirac carriers $\epsilon_k = v_F\hbar k$, and using $\int_0^{2\pi}\cos^2(\theta)d\theta = \pi$ the integral becomes:

$$\frac{e^2E}{\pi\hbar^2}\int\epsilon d\epsilon[-\frac{\partial f^m(\epsilon_\mathbf{k},x,t)}{\partial\epsilon_\mathbf{k}}] = (\gamma+\frac{\partial}{\partial t})J \tag{88}$$

and in the low temperature limit $T\to 0$, $-\frac{\partial f^m(\epsilon_\mathbf{k},x,t)}{\partial\epsilon_\mathbf{k}}\to\delta(\epsilon-\epsilon_F(x,t))$, so that we get:

$$\frac{e^2}{\pi\hbar^2}\epsilon_F(x,t)E = (\gamma+\frac{\partial}{\partial t})J \tag{89}$$

The electric field is $E(x,t) = e^{i(qx-\omega t)}\sum_n E_n e^{in(gx-\Omega t)}\hat{\mathbf{x}}$, and we seek a Floquet-Bloch solution for the current $J(x,t) = e^{i(qx-\omega t)}\sum_n J_n e^{in(gs-\Omega t)}$ [2], so that:

$$\frac{e^2\epsilon_{F,0}}{\pi\hbar^2}\sum_{n'}[e^{in'(gx-\Omega t)}+\alpha(e^{i(n'+1)(gx-\Omega t)}+e^{i(n'-1)(gx-\Omega t)})]E_{n'} = \sum_m[\gamma-i(\omega+m\Omega)]J_m e^{im(gx-\Omega t)} \tag{90}$$

Finally, multiplying by $e^{-in(gx-\Omega t)}$, integrating, and solving for J_n:

$$J_n = \frac{e^2\epsilon_{F,0}}{\pi\hbar^2}\frac{[E_n+\alpha(E_{n+1}+E_{n-1})]}{\gamma-i\omega+n\Omega} \tag{91}$$

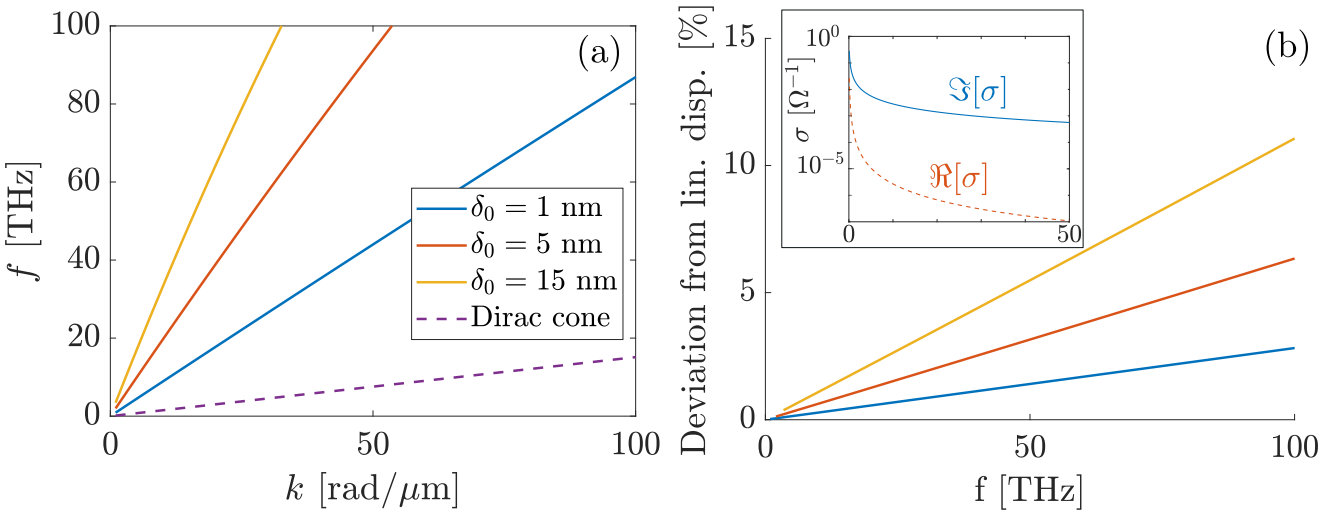

Figure 3: (a) Dispersion relation of acoustic plasmons in DLG for different values of the interlayer gap δ_0. (b) Deviation of the acoustic plasmon dispersion from the linear regime (in percentage) for different values of δ_0. The inset shows the reactive (imaginary, continuous blue line) and dissipative (real, red dashed line) parts of the conductivity as a function of frequency.

6 Dispersion relations of acoustic plasmons in DLG

In the interest of completeness, we report here (Fig. 3a) the dispersion relation of acoustic plasmons in graphene:

$$\omega = \left(\frac{e^2 \epsilon_F}{2\varepsilon_0 \hbar^2} k(1 - e^{-k\delta_0}) \right)^{1/2} \tag{92}$$

for different values of the interlayer gap $\delta_0 = 1$ (blue curve), 5 (red curve) and 15 nm (yellow curve), together with the Dirac cone (purple dashed line) $f = v_F k/(2\pi)$ [1].

Furthermore, we show in Fig. 3b the % deviation of the frequency of acoustic plasmons from the linear regime $e^{-k\delta_0} \simeq 1 - k\delta_0$, as a function of frequency, for the same values of the interlayer gap.

Finally, the inset shows the reactive (imaginary, continuous blue line) and dissipative (real, red dashed line) parts of the Drude conductivity of graphene for the parameters used in the main text:

$$\sigma(\omega) = \frac{e^2}{\pi \hbar^2} \frac{\epsilon_F}{\gamma - i\omega} \tag{93}$$

References

[1] Paulo André Dias Gonçalves and Nuno MR Peres. *An introduction to graphene plasmonics*. World Scientific, 2016.

[2] Edward S Cassedy. Waves guided by a boundary with time—space periodic modulation. In *Proceedings of the Institution of Electrical Engineers*, volume 112, pages 269–279. IET, 1965.

[3] T Stauber, NMR Peres, and F Guinea. Electronic transport in graphene: A semiclassical approach including midgap states. *Physical Review B*, 76(20):205423, 2007.